the plant journal

SEB Society for Experimental Biology

The Plant Journal (2017) **90,** 204–216 doi: 10.1111/tpj.13472

TECHNICAL ADVANCE

Phenotiki: an open software and hardware platform for affordable and easy image-based phenotyping of rosette-shaped plants

Massimo Minervini[1], Mario V. Giuffrida[1,2,3], Pierdomenico Perata[4] and Sotirios A. Tsaftaris[2,*]

[1]*IMT School for Advanced Studies, Piazza S. Francesco 19, 55100 Lucca, Italy,*

[2]*Institute for Digital Communications, School of Engineering, University of Edinburgh, Thomas Bayes Road, EH9 3FG Edinburgh, UK,*

[3]*The Alan Turing Institute, 96 Euston Road, NW1 2DB London, UK, and*

[4]*PlantLab, Institute of Life Sciences, Scuola Superiore Sant'Anna, Via Mariscoglio 34, 56124 Pisa, Italy*

Received 25 May 2016; revised 21 November 2016; accepted 22 December 2016; published online 9 January 2017.
*For correspondence (e-mail S.Tsaftaris@ed.ac.uk).

SUMMARY

Phenotyping is important to understand plant biology, but current solutions are costly, not versatile or are difficult to deploy. To solve this problem, we present Phenotiki, an affordable system for plant phenotyping that, relying on off-the-shelf parts, provides an easy to install and maintain platform, offering an out-of-box experience for a well-established phenotyping need: imaging rosette-shaped plants. The accompanying software (with available source code) processes data originating from our device seamlessly and automatically. Our software relies on machine learning to devise robust algorithms, and includes an automated leaf count obtained from 2D images without the need of depth (3D). Our affordable device (~€200) can be deployed in growth chambers or greenhouse to acquire optical 2D images of approximately up to 60 adult Arabidopsis rosettes concurrently. Data from the device are processed remotely on a workstation or via a cloud application (based on CyVerse). In this paper, we present a proof-of-concept validation experiment on top-view images of 24 Arabidopsis plants in a combination of genotypes that has not been compared previously. Phenotypic analysis with respect to morphology, growth, color and leaf count has not been performed comprehensively before now. We confirm the findings of others on some of the extracted traits, showing that we can phenotype at reduced cost. We also perform extensive validations with external measurements and with higher fidelity equipment, and find no loss in statistical accuracy when we use the affordable setting that we propose. Device set-up instructions and analysis software are publicly available (http://phenotiki.com).

Keywords: phenotyping, *Arabidopsis thaliana*, growth, software, image analysis, affordable, Raspberry Pi, technical advance.

INTRODUCTION

The plant research community appreciates the need to rapidly phenotype, in a reliable fashion, the growth of plants. Having an in-depth understanding of such information could help us to identify suitable traits to be used for breeding new crops. Model plants, such as *Arabidopsis thaliana*, combined with quantitative information obtained manually or via observation, have become an invaluable tool in this quest (Furbank and Tester, 2011). Recently, the introduction of digital imaging and automation have radically changed how phenotypes are described (Rousseau *et al.*, 2015), in model plants and in general. Experts can analyze the images offline (i.e. at a later point in time after the actual plant experiment), disentangling the process of imaging (sensing) from phenotype analysis. With image analysis this process has been further simplified (Sozzani *et al.*, 2014), and the labor effort has been significantly

reduced, to the point that automated phenotyping is now sought-after by many laboratories around the world in an attempt to relieve the phenotyping bottleneck (Furbank and Tester, 2011).

As a result, several phenotype acquisition approaches have emerged that can be broadly categorized as those relying on commercial equipment (e.g. LemnaTec, http://www.lemnatec.com; CropDesign, http://www.cropdesign.com; Phenospex, http://phenospex.com; Photon Systems Instruments, http://www.psi.cz) or custom-built solutions that may rely on affordable (e.g. Leister *et al.*, 1999; Tsaftaris and Noutsos, 2009; Bours *et al.*, 2012; De Vylder *et al.*, 2012; Green *et al.*, 2012) or costly imaging sensors coupled with actuation (Granier *et al.*, 2006; Walter *et al.*, 2007; Jansen *et al.*, 2009; Tisné *et al.*, 2013; Brown *et al.*, 2014; Apelt *et al.*, 2015). Both approaches have a key limitation: a high entry barrier, as a result of cost or difficult deployment and maintenance, or the lack of a robust and expandable software platform. This has hindered the widespread adoption of image-based technologies as a practical and standard tool in plant phenomics for the common lab.

In this paper we propose Phenotiki, an affordable and yet practical approach to the phenotyping of rosette-shaped plants that is easy to install and deploy, and is accompanied by robust, free (with available source code) software.

Phenotiki (Figure 1) combines an imaging device with a complete, open, expandable stand-alone software package (Figure S3), designed to offer an out-of-box experience when used together. To be affordable (less than €200), easy to deploy, use and maintain, no moving parts are used and all hardware is easy to source as it is based on the Raspberry Pi platform. The software system offers automated or semi-automated analysis of several visual phenotypes, based on a wide range of traits, ranging from typical size and growth descriptors to color and even leaf count. Our imaging device is tasked with taking images, and we offer software that runs on the device to enable easy programmatic control. Analysis (and data storage) occurs at local workstations or via the web browser in the Cloud. Our analysis software, to be reliable when used in different laboratories (or even with other imaging systems), integrates analysis algorithms based on state-of-the-art methods of image processing and machine learning that have appeared in engineering conferences and journals, passing the technical scrutiny of the audience at these venues (Minervini *et al.*, 2014, 2015a; Giuffrida *et al.*, 2015). Notably, we include machine learning-driven methods for: (i) automated plant segmentation from tray images (Minervini *et al.*, 2014); (ii) semi-automated interactive leaf segmentation (Minervini *et al.*, 2015a); and (iii) automated leaf counting (Giuffrida *et al.*, 2015), all within the confines of affordable 2D-based vision without the need for costly 3D cameras (Apelt *et al.*, 2015).

To demonstrate the phenotyping potential of Phenotiki, we present results from a proof-of-concept experiment containing several replicates of Arabidopsis (wild-type and mutants) that were imaged simultaneously. We characterized the accuracy of the system with traditional manual measurements and other (costlier) imaging sensors. Several statistical experiments on extracted growth, morphological and color phenotypes confirmed that Phenotiki can phenotype at a remarkably reduced cost.

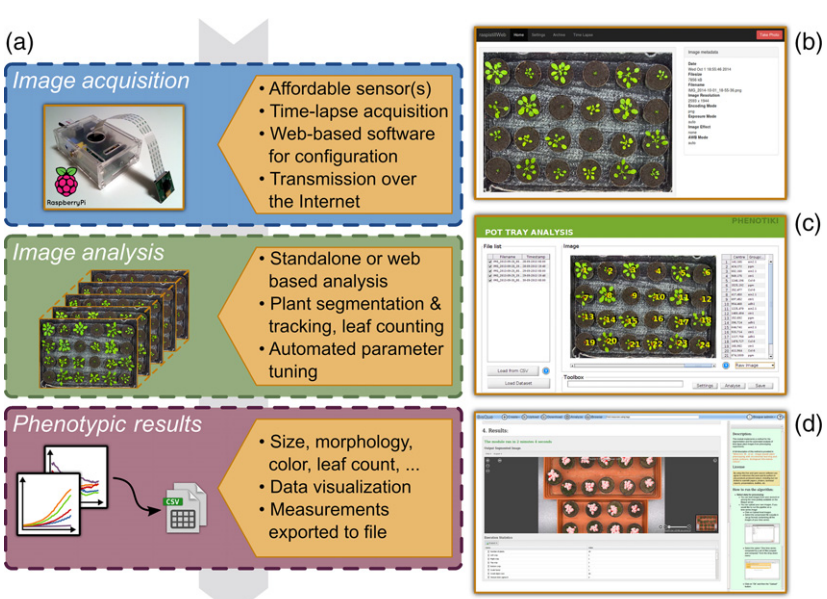

Figure 1. Overview of the Phenotiki system and screen captures showing the graphical user interfaces to operate its hardware and software components. (a) Schematic of the proposed distributed sensing and analysis framework illustrating the main components of our phenotyping platform. (b) Web interface to configure and operate the Phenotiki device from the browser. (c) Stand-alone version of the image-analysis software. (d) Cloud-based version of the image analysis software that runs on a web browser. [Colour figure can be viewed at wileyonlinelibrary.com].

RESULTS

Plant material

The experiment involved 24 *A. thaliana* plants, including the wild type (ecotype Col-0) and four different mutants, all in the Col-0 background, with an arrangement as shown in Figure 2(b). The *constitutive triple response 1* (*ctr1*; Kieber *et al.*, 1993) and *ethylene insensitive 2* (*ein2.1*; Guzmán and Ecker, 1990) are defective in ethylene signaling. The *pgm* mutant is unable to accumulate transitory starch as a consequence of a mutation in the plastidic isoform of the phosphoglucomutase (*PGM*), which is required for starch synthesis (Caspar *et al.*, 1985). The *adh1* mutant is defective in alcohol dehydrogenase activity, an enzyme playing an essential role in plant tolerance to hypoxia (Perata and Alpi, 1993). Although *pgm* and *ctr1* are well known to display reduced growth, *ein2.1* and *adh1* mutations do not have a major impact on growth, at least based on the original reports describing these mutants. The *ctr1* mutant constitutively displays phenotypes associated with ethylene signaling, the consequences of which include extreme dwarfism (Kieber *et al.*, 1993). The *ein2.1* mutant, which is insensitive to ethylene, instead displays minor phenotypic differences when compared with the wild type, although it has been reported to grow slightly bigger (Guzmán and Ecker, 1990). The *pgm* mutant is smaller than the wild type (Caspar *et al.*, 1985). Interestingly, the growth of a similar mutant (starch-free 1; *stf1*) was recently studied by digital imaging, providing an interesting benchmark for our study (Wiese *et al.*, 2007). Further details on growth conditions are provided in the Experimental procedures.

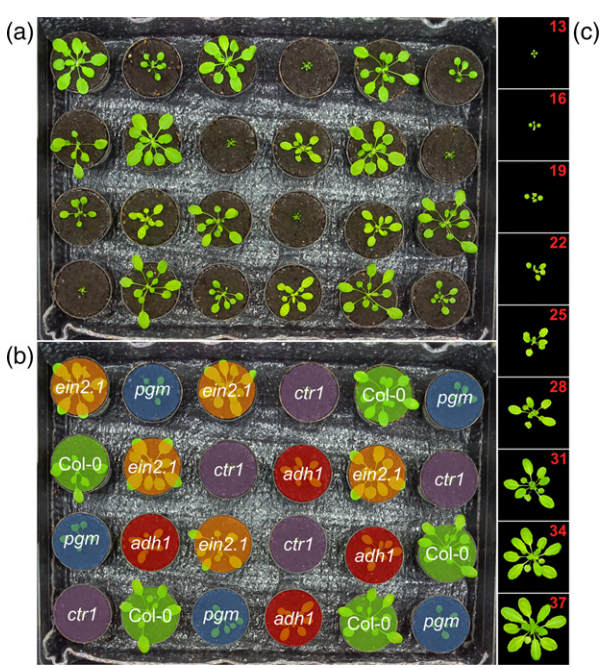

Figure 2. Example imaging data acquired by the Phenotiki system. (a) Original image and (b) illustration of the randomized arrangement of the genotypes in the scene. (c) A growing *adh1* subject at different stages (numbers in red denote days after sowing), with the plant delineated via automatic segmentation (Minervini *et al.*, 2014). [Colour figure can be viewed at wileyonlinelibrary.com].

Brief overview of the Phenotiki system

Phenotiki is composed of an affordable image-acquisition device (of less than €200 in material cost) and a suite of (stand-alone or web-based) software tools for image analysis. The architecture of Phenotiki is illustrated in Figure 1.

The Phenotiki device consists of a Raspberry Pi embedded computer (http://www.raspberrypi.org) operating the RaspiCam fixed-focus (and fixed-zoom) imaging sensor. As Figure S1 shows, the device is small (10 × 6.5 × 3.5 cm) and lightweight (115 g), and it was affixed with zip ties to the ceiling of the growth chamber. The device was enclosed in plastic housing (Figure S1) and could wirelessly connect to the Internet after it was set up (a complete equipment list is provided in Appendix S1). We devised graphical software (Figures 1b and S2; Video clip S1) for ease of interaction with the device, which allowed us to define an acquisition schedule and parameters for time-lapse 2D optical imaging of the scene and data transmission. Phenotiki was calibrated and configured to acquire top-view images (Figure 2a) with a preset time schedule (every 12 h, respectively, at the beginning and the end of the 12-h photoperiod) and fixed imaging conditions (e.g. focus, exposure, field of view) over a period of 26 days, resulting in a time-lapse sequence of 52 images in total.

Data storage and processing were decoupled from acquisition. Image data can be transmitted over the local network or the Internet to a centralized repository (on site or remote) for analysis. Our device can also directly connect to CyVerse (formerly iPlant Collaborative, http://www.cyverse.org) to upload data, and using our modules built upon the BisQue framework (Goff *et al.*, 2011) can offer a Cloud-based application to store and analyze the images for higher throughput potential (see Appendix S2 for the naming of modules on CyVerse). For this paper, results were obtained based on the stand-alone software after imaging data were collected at a local workstation.

The same software base is used in both the stand-alone and the Cloud applications (screen shots shown in Figures 1c,d, S3 and S4; usage demonstrated in Video clips S2 and S3). Robust (and validated) image processing algorithms have been efficiently implemented to enable annotation, detection, tracking and segmenting plants from the background (Minervini *et al.*, 2014), and also counting leaves automatically (Giuffrida *et al.*, 2015). These are available as modules that can be either used through the stand-alone graphical interface (Figure S3) or in the web-based application (Figure S4). This design also

demonstrates how our platform can be extended to address future hypotheses.

We obtained phenotypic information related to plant growth, morphology, color and leaf count. Measurements were exported from our software in machine-readable format and were imported to MATLAB (http://mathworks.com) and R (http://www.r-project.org) for visualization and statistical analysis. The plant segmentation and leaf-counting components of our system can operate autonomously on large data sets once they have been configured. Before analyzing the entire data set for plant growth, we annotated one image (i.e. delineating the plants from the background, a task that can be completed efficiently with the aid of our semi-interactive annotation tool, described in detail in Appendices S2 and S3), on the basis of which optimal operational parameters were found automatically by our software through an optimization process, thus eliminating the need for the user to trial parameters. The same parameters were applied to the entire image sequence of the experiments presented herein. We also used annotations of the number of plant leaves for a set of representative training images to learn a model that can estimate the leaf count of unseen images, and then applied this model to the entire data set.

Software and sensor set-up instructions are in the public domain at http://phenotiki.com. Further details on imaging set-up, computer vision approaches and the definition of the scored visual traits (see also Figure S5) are provided in the Experimental procedures section and in Appendices S2–S4. Measurement validation with non-image measurements and comparison with a higher-grade camera follow the presentation of phenotypic findings.

Phenotypic results

Phenotyping plant area and morphology. We compared the rosette size achieved by different genotypes based on projected leaf area (PLA), diameter and perimeter. Results are shown in Figure 3(a,c,d). Separate repeated-measures ANOVA with the Greenhouse–Geisser correction were used to assess the effects on each of the descriptors of time (within-subject factor), genotype (between-subject factor) and their interaction. For all three descriptors there was a significant time–genotype interaction ($P < 0.01$). Tukey–Kramer's multiple comparison ($P < 0.05$) revealed that three distinct groups can be identified: Col-0 and *ein2.1* presented the largest size; *adh1* and *pgm* presented medium size; and *ctr1* exhibited extreme dwarfism, and hence the smallest size. These results were expected for *pgm* (Caspar *et al.*, 1985; Apelt *et al.*, 2015) and *ctr1* (Kieber *et al.*, 1993). In the case of *ein2.1*, a larger plant diameter was previously reported for 24-day-old plants (Guzmán and Ecker, 1990), whereas our data showed a plant diameter slightly smaller than the wild type in the case of *ein2.1* (Figure 3c). No obvious phenotypes were previously reported for *adh1* mutants. Since the enzyme ADH is involved in hypoxia tolerance it is tempting to speculate that the adopted watering plan (twice a week by sub-irrigation for all plants) might have led to root hypoxia for *adh1* mutants, which are more sensitive to watering level, with consequences on plant growth.

Compactness data did not suggest any evident groupings (Figure 3e); however, note that *ein2.1* presented higher compactness than Col-0 ($P < 0.01$, paired Student's *t*-test), although they shared similar size. Higher stockiness was consistently observed for *ctr1* with respect to the other genotypes (Figure 3f), although this may partly result from the considerably smaller size of the *ctr1* plants and fixed (per plant) imaging resolution, so that the extremely dwarf plants will appear concentrated and more circular.

We also adopted a parametric model-driven approach to growth analysis based on Richards' growth curve (Appendix S5) and observed PLA data, the result of which is shown in Figure S6 and Table S1. Average normalized growth rates indicated slower growth for *ctr1* and *pgm* with respect to the other genotypes. In fact, the time of inflection in the growth curves (γ) of *ctr1* and *pgm* was estimated, respectively, at approximately 42 and 36 days after sowing, whereas this was 30 days after sowing for the wild type. Finally, based on 95% confidence intervals for the estimated value of parameter *k*, we observed that the growth rate of *pgm* was significantly lower than Col-0, *ein2.1* and *adh1*.

Phenotyping growth stage based on leaf counting. We also compared leaf-counting progression (Figure 4a) and developmental growth stages among genotypes, identified by the number of leaves, based on the scale discussed in Boyes *et al.* (2001). In Figure 4(b) we highlight which day after sowing a group of plants (i.e. genotype) developed four leaves (1.04), 10 leaves (1.10), 14 leaves (1.14) and later leaf-related stages (>1.14), respectively. In accordance with the previous analysis based on plant size, we observe that *ein2.1* and Col-0 reached successive growth stages more rapidly than the other genotypes, with *pgm* and *ctr1* producing new leaves at a markedly slower pace than the wild type. A pairwise Tukey–Kramer comparison (following a significant repeated-measures ANOVA) on leaf count data, as plotted in Figure 4(a), confirmed that *adh1*, *pgm* and *ctr1* differed from the wild type ($P < 0.05$, cf. Table S3).

Phenotyping diel growth dynamics. Differences in diurnal and nocturnal growth rates were assessed based on the average (aggregated throughout the experiment) relative growth rate (RGR), using a one-way ANOVA followed by Tukey–Kramer multiple comparison amongst the five groups, with the results shown in Figure 5. Overall, considering a diel growth cycle, *ctr1* presented a lower RGR than the other genotypes ($P < 0.01$). Also *ein2.1* had a lower growth rate than the control ($P < 0.05$). When considering

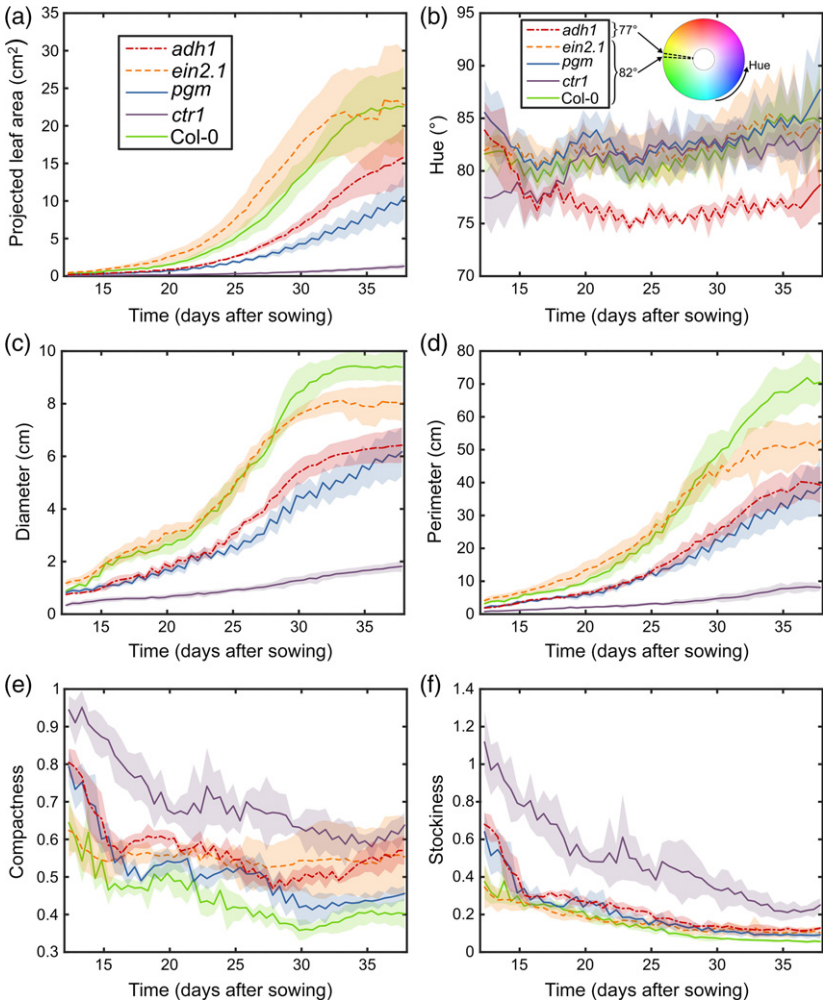

Figure 3. Plant size, morphology and color (hue) traits (*y*-axis) plotted against time (*x*-axis). Measurements were taken for 25 days every 12 h. Genotypes are identified by color and variance is denoted by shaded areas. The legend in panel (a) applies to all panels. To improve the clarity of visualization of panel (b), a third-order Savitzky–Golay smoothing filter with a kernel size of seven was applied to each time series. Also shown is the HSV (hue, saturation and value) color wheel, with values for H ranging from 0 to 360°, and an indication of the average value for *adh1* (77°) and for the other four genotypes collectively (82°). [Colour figure can be viewed at wileyonlinelibrary.com].

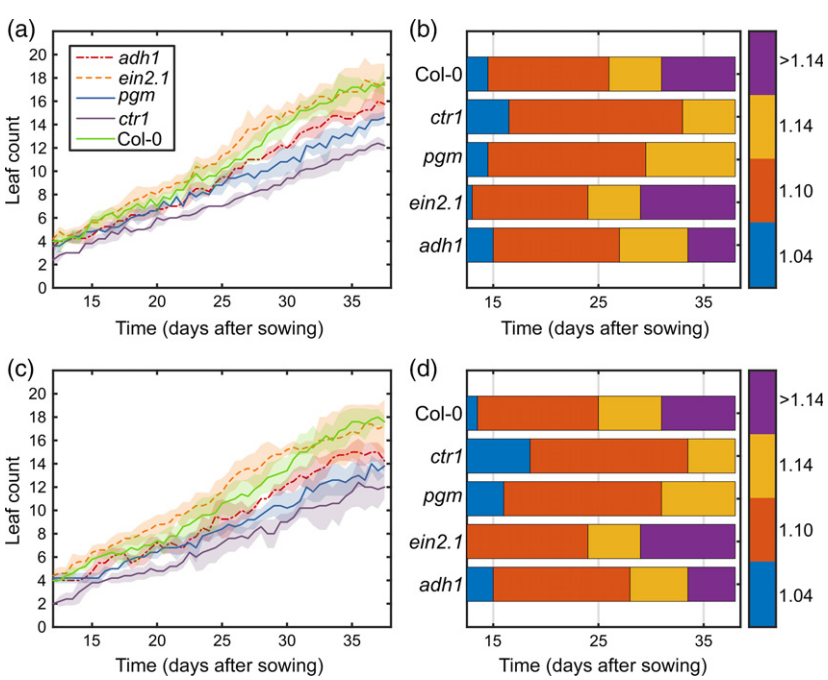

Figure 4. Leaf-counting data (a, b), estimated by our automated leaf-counting algorithm and (c, d) derived from the expert annotations. Results are shown as (a, c) time-series plots and (b, d) growth progression bars (Boyes *et al.*, 2001). The learning-based counting algorithm was trained on a subset of plant images and then applied to the entire data set. [Colour figure can be viewed at wileyonlinelibrary.com].

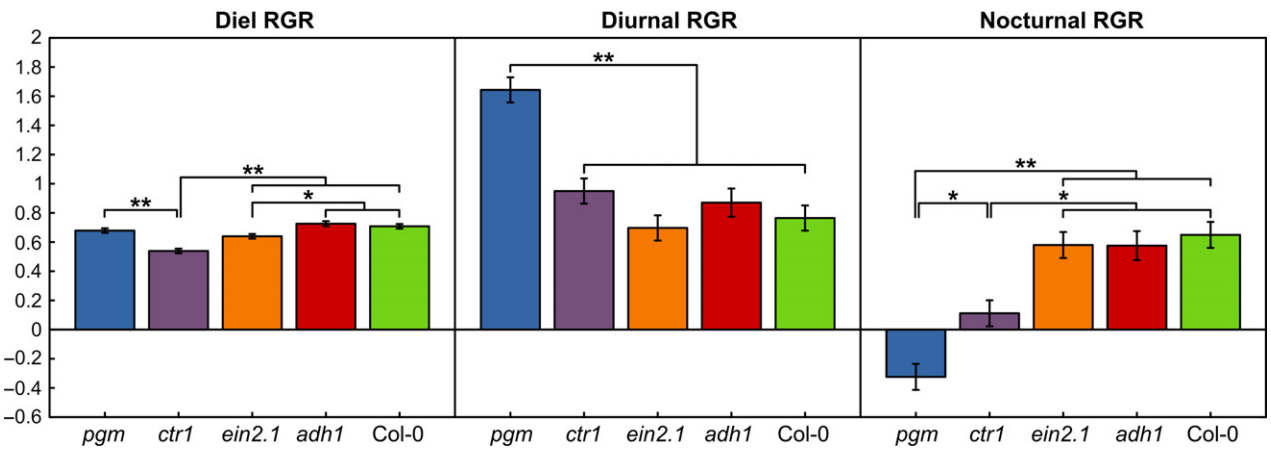

Figure 5. Average relative growth rate (RGR) by genotype across the duration of the study (from 12 to 37 days after sowing). Shown are, respectively, diel, diurnal and nocturnal RGR. Data are represented as means ± standard errors of the mean. The lines and asterisks above the bars indicate statistically significant differences in average RGR between genotypes, as determined by Tukey–Kramer multiple comparisons test (*$P < 0.05$; **$P < 0.01$). [Colour figure can be viewed at wileyonlinelibrary.com].

diurnal growth, *pgm* exhibited a considerably higher (approximately double) growth rate than the other genotypes ($P < 0.01$). During night-time, growth of *pgm* decreased considerably. Reduced nocturnal growth was previously reported by Wiese *et al.* (2007) using the *stf1* mutant that, as in the case of *pgm*, is defective in the plastidial phosphoglucomutase enzyme. Differences in diurnal and nocturnal growth rates within a genotype were assessed via paired Student's *t*-test, which was significant for *pgm* and *ctr1* ($P < 0.01$), showing preferential growth during the day, and also for *adh1* ($P < 0.05$). On the other hand, no significant difference in diurnal and nocturnal RGR was observed for *ein2*.1 and Col-0. Daily cyclic patterns as evident in Figure 3 were also demonstrated by power spectral density estimation of the PLA data (Figure 3a) shown in Appendix S6.

Phenotyping color. The color of plant subjects was in general bright green, and after an initial adjustment it did not vary significantly throughout the experiment (Figure 3b). On the other hand, a comparison among groups revealed that the color of *adh1* statistically differed from the other genotypes. We measured color changes quantitatively using the HSV (hue, saturation and value) color space. On average, the color of *adh1* (hue = 77°) differed from all other genotypes (hue = 82°), with a drift towards yellow hues (Figure 3b), as highlighted by a repeated-measures ANOVA followed by Tukey–Kramer multiple comparison ($P < 0.01$). The yellowish color of *adh1* again suggests that the plants suffered from root hypoxia, and this trait was found by our analysis based on Phenotiki.

Measurement validation

Validating plant growth measurements. Central to measuring plant growth with our software is the algorithm for delineating (segmenting) the plants from the background. Whereas previously the plant segmentation algorithm has been validated against manual image-based plant delineations, showing 97% overlap agreement (Minervini *et al.*, 2014), here we compare its performance with the traditional non-image-based measurement approach, as performed by others (De Vylder *et al.*, 2012). Specifically, we recorded the diameter of each subject measured on a daily basis at the end of the photoperiod using a digital caliper, obtaining 360 manual measurements overall. Those were compared with image-based calibrated values obtained automatically using our software on the corresponding images. The scatter plot in Figure 6(a) shows excellent agreement between automatic and manual measurements, with a concordance correlation coefficient for repeated measures of $\rho_{CCC,RM} = 0.997$ (lower 95% confidence limit = 0.995), which is proper for longitudinal studies when within-subject correlation may exist as a result of repeated measures (Carrasco *et al.*, 2013). Additionally, the quantile–quantile plot in Figure 6(b) shows that measurements obtained with the two methods follow similar distributions. To demonstrate that our accuracy is consistent across measurement range, the Bland–Altman (B–A) plot in Figure S7 compares measurement difference with the mean for each pair of observations. The B–A analysis was conducted with the method described by Bland and Altman (2007), which accounts for repeated measures. The average measurement was 3.655 cm and given the small bias of −0.048 cm, and 95% limits of agreement (mean difference ± 1.96 SD) from −0.394 to 0.298 cm, we can conclude that automatic and manual measurements of rosette diameter were in excellent agreement.

Comparison with a higher grade camera with optical zoom. The Phenotiki device uses the RaspiCam fixed-

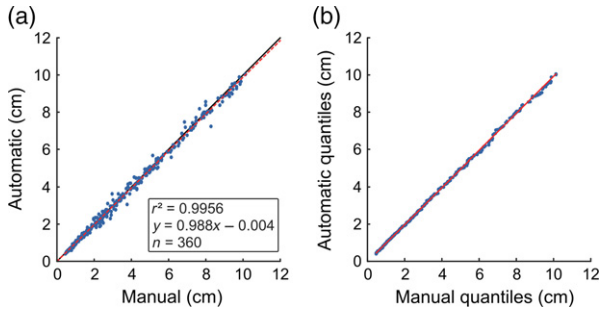

Figure 6. Agreement between rosette diameter measured from images using Phenotiki (automatic) and manually with a caliper (manual). (a) Scatter plot with fitted linear regression (dashed red line) and 45° rising line (black solid line). (b) Q–Q plot with superimposed red line joining the first and third quartiles of each distribution. [Colour figure can be viewed at wileyonlinelibrary.com].

focus camera to acquire images of the scene. With the absence of moving parts and focusing options, cameras with fixed focus are cheaper and easier to set than those with autofocus or manual focus; however, the latter in general provide higher-quality images. To assess whether such higher quality provides any additional benefits (e.g. higher statistical power) for a similar phenotyping experiment to ours, we also used a more expensive consumer-grade Canon camera with movable optics, which has a higher effective resolution because of the movable lens (zoom), but was also placed to image at an effective field of view assuming imaging at 50 cm (typical of a growth shelf). To permit the comparison, the Canon was installed alongside the RaspiCam, to take images of the same plants and arrangement at exactly the same time of the day.

First, we validated the Canon sensor against manual measurements of rosette diameter. Repeating the same regression and B–A type analyses as described previously, no differences were found in measurement accuracy with manual measurements (Figure S8). Comparing limits of agreement and bias between the Canon and the RaspiCam, differences were minimal (Figures S7 and S8), indicating that there was no difference between the two camera sensors with respect to manual measurements.

We repeated all the phenotypic analyses described in the previous section using images from the Canon camera. In all cases we observed agreement on the statistical differences already found using the RaspiCam. As an example, Table S2 compares the results of the pairwise Tukey–Kramer comparison (following a significant repeated-measures ANOVA) between PLA data of different genotypes obtained with RaspiCam and Canon sensors, respectively. Observe that the *P* values are close to each other and at a significance level of 0.05 the conclusions are the same.

Finally, to determine whether sensor quality was a factor we pooled PLA data measured respectively by RaspiCam and Canon, and added camera type as an additional factor to the above ANOVA setting. We found that the camera type was insignificant ($P = 0.696$).

Validating leaf counting. To automatically estimate the number of plant leaves in 2D images without 3D information, we devised a machine vision algorithm that predicts the number of leaves based on plant features in the images that are learned in a data-driven fashion (Giuffrida *et al.*, 2015).[1] For the purpose of this validation experiment all image data were labeled by a human expert (with the use of the annotation tool) to associate the number of leaves in each of the 1248 plant images in our data set, which was then used to train and evaluate the method.

Figure 4 shows the time series of the number of leaves for each genotype (Figure 4c) and growth progression bar (Figure 4d), as derived from the expert annotations. One can readily observe that growth trends are in agreement between predicted and ground-truth (expert) counts (Figure 4a,c). This is also evident when visualized with growth progression bars (Boyes *et al.*, 2001) of the predicted (Figure 4b) and expert-derived data (Figure 4d), demonstrating that our algorithm can detect the specific growth stages of a plant (principal growth stage 1; Boyes *et al.*, 2001).

Quantitative analysis is shown in Table 1, reporting four (now standard) evaluation metrics (Scharr *et al.*, 2016), which compare agreement between the ground-truth and the predicted count as: difference in count (*DiC*), absolute difference in count (|*DiC*|), mean squared error (*MSE*) and coefficient of determination (R^2). With respect to the algorithm presented in Giuffrida *et al.* (2015), Phenotiki adopts an extended version that relies on image features and also plant genotype and projected leaf-area variables to estimate the number of leaves (further details can be found in the Experimental procedures). The results produced by the algorithm agree with leaf counts made by expert inspectors ($R^2 = 0.94$ on the testing set), with mean and standard deviations of less than 1 in absolute count (|*DiC*|). Automated leaf counts differed from an expert's manual count by not more than one leaf in 83% of examples.

As a further validation, we evaluated whether interchanging the expert data with the automated predictions had any effect in statistical comparison testing. Table S3 compares the results of the pairwise Tukey–Kramer comparison (following a significant repeated-measures ANOVA) between count data of different genotypes obtained with the expert data and the automated counting, respectively. Observe that the *P* values are close to each other and at the 0.05 significance level the phenotypic conclusions are the same.

[1]An earlier version of this algorithm won the first place in the 2015 edition of the Leaf Counting Challenge (http://www.plant-phenotyping.org/CVPPP2015-challenge).

Table 1 Quantitative performance of the leaf counting algorithm in Phenotiki

	Phenotiki		Giuffrida *et al.* (2015)	
	Training	Testing[a]	Training	Testing
DiC	**0.032 ± 0.772**	**0.186 ± 0.995**	0.107 ± 1.171	0.247 ± 0.1.428
|*DiC*|	**0.580 ± 0.509**	**0.702 ± 0.728**	0.880 ± 0.779	1.048 ± 1.000
MSE	**0.596**	**1.022**	1.380	2.096
R^2	**0.967**	**0.939**	0.926	0.876

We compared the original algorithm described in Giuffrida *et al.* (2015) and the extended version proposed in this article. Difference in count (*DiC*), absolute difference in count (|*DiC*|), mean squared error (*MSE*) and coefficient of determination (R^2). Lower *DiC*, |*DiC*| and *MSE* are better, whereas higher R^2 is better. The best results are highlighted in bold.

These data, following typical practice in machine-learning literature, reflect performance under a random sampling of the sets that we train on and test on. We follow a strict subject-out 50% split of the complete data. The data set includes 24 plants imaged for 26 days. The data set is split into two halves, randomly selecting 12 plants each time (and all the pictures of a plant across time) as a training set and the remaining 12 plants as a testing set (used to assess generalization error), ensuring that both subsets include examples of all genotypes (Col-0, *adh1*, *ctr1*, *ein2.1* and *pgm*). Hence the values of *DiC* and |*DiC*| reflect the average and the standard deviation on each set, whereas *MSE* and R^2 are, by definition, aggregates.

[a]If we are to repeat this random split many times (in machine learning this is a form of cross-validation) we see that performance remains the same, with average and standard deviations of the same measurements as 0.041 ± 0.154 (*DiC*), 0.841 ± 0.067 (|*DiC*|), 1.335 ± 0.180 (*MSE*), 0.923 ± 0.008 (R^2). This indicates stability with respect to the set that we train on.

DISCUSSION

We presented an affordable and easy to use solution to plant phenotyping. It was validated using a proof-of-concept phenotyping experiment with Arabidopsis genotypes (some of which with known growth characteristics) to demonstrate that, despite the employment of low-cost hardware, it can characterize growth in a satisfactory fashion. The system was validated extensively using non-image-based methods via measuring rosette diameter with a caliper and also using expert annotation of the images via manual counting of plant leaves. The underlying plant segmentation algorithm has also been previously validated with manual delineations of plants (Minervini *et al.*, 2014). Furthermore, it was also compared with a higher-grade camera that had movable optics. Overall, we found no significant differences between the measurements obtained with our system and those obtained by other means.

We adopted a distributed design and decoupled sensing from analysis and storage. This lowered the cost of the device and provides scalability. We rely on an off-the-shelf embedded computer (the Raspberry Pi) and a fixed-optics camera sensor for several reasons. The Raspberry Pi is affordable and offers sufficient computational power; furthermore, it has a large following and a vast user and development community, and several core suppliers. This credit-card sized yet complete computer attached to the imaging sensor can be used for storage (i.e. the device can serve even as simple data logger), but is used in Phenotiki to control the imaging sensor and transmit data to the computational unit. The fixed-optics sensor offers robustness to environmental conditions by reducing condensation effects with the lack of movable parts; alternatively, moving optics cameras require expensive housing to protect against condensation.

Our device can be set up in less than 1 day. Hardware components can be easily obtained from one of the many suppliers. Additional step-by-step instructions on assembling and installing the device and software are available on the Phenotiki website (http://phenotiki.com).[2] This also installs the software that allows the control and set up of the imaging settings via web-based interface. In addition, it provides guidelines for the calibration processes. The device can be attached to growth chambers or shelves and requires a single cable for power. Once installed it can operate unattended with the same imaging parameters and requires virtually no maintenance when not displaced. This level of technology readiness is unprecedented for an affordable, yet integrated, plant phenotyping system.

With its small footprint, the device easily fits in a growth chamber and does not cover much of the chamber lights. For example, by installing it 1 m above the plants, the camera ensures a field of view of 0.5 m^2, which would permit the imaging of about 60 Arabidopsis plants grown in pots throughout their life cycle, with an imaging resolution suitable for the phenotyping applications shown in this article. Equivalently, when placed 50 cm above the plants, the device can image approximately 30 subjects, offering even higher resolution. Informal discussions with several plant scientists confirmed that this is adequate when pilot

[2]We maintain software and user manuals at an external repository to permit their continuous updating.

studies are sought after. The system can reach higher throughput while still maintaining affordability by increasing the number of sensors: because of its compact size and low cost, multiple Phenotiki devices can be readily deployed to offer even higher imaging resolution or throughput. Thus we avoid complex and costly solutions based on robotics and actuation (as for example in Tisné *et al.*, 2013), which typically have a larger footprint reducing further the already hard to find growth chamber space, and require specific know-how and maintenance, necessitating additional in-house expertise (which may not be available at length) or service contracts (when development has been outsourced).

The imaging data acquired by the device are sent to a local workstation or to the Cloud. The on-site data hosting and processing on a workstation is ideal for laboratories with expected small throughput, and for users who prefer to rely on local, in-house computational infrastructure. On the other hand, our distributed approach permits us to outsource storage and computation to the Cloud, thus relieving the user from the cost of purchasing and maintaining a high-performance computing infrastructure *in situ* when throughput will be high. Furthermore, by relying on the Cloud, the additional computational needs to analyze higher throughput data can be readily met because of its immediate resource scalability, and the implementation of asynchronous upload mechanisms that are used by our device to send data to the Cloud. When the available network bandwidth or storage capacity is limited (which could occur in laboratories in countries with poorer Internet infrastructure), we can potentially integrate image compression algorithms within the Phenotiki device (Minervini and Tsaftaris, 2013; Minervini *et al.*, 2015c).

Our analysis software and graphical interface are built on top of MATLAB and are publicly available to the academic community. We provide pre-compiled versions of the software that do not require a MATLAB installation or license, and can be executed as a stand-alone program. Our source code is also available to permit third-party extensions. For those that do not want to rely on local processing, image analysis modules of Phenotiki for plant segmentation and annotation are available on the BisQue platform provided by CyVerse (Goff *et al.*, 2011). Our interface is intuitive and our software is designed in a modular fashion, such that new analysis pipelines can be integrated.

Most of the available software packages for plant phenotyping (http://plant-image-analysis.org; Lobet *et al.*, 2013) are tuned to specific set-ups and assumptions. Instead, we wanted to create software that potentially can be adopted in a variety of experimental settings anticipating that it will be used in several laboratories. This necessitates image-processing algorithms that are adaptable. Approaches that rely on constraining the experimental setting and applying thresholds on image intensity values (e.g. De Vylder *et al.*, 2012; Easlon and Bloom, 2014) are not readily portable across different labs because they offer limited robustness to varying conditions (e.g. changes in plant appearance as a result of senescence or treatment), changes in illumination (e.g. different daylight conditions) or unplanned alterations in the background (e.g. algae growing on soil). In fact, the need for robust image-analysis algorithms and software has been labeled as the new bottleneck in plant phenotyping (Minervini *et al.*, 2015b; Tsaftaris *et al.*, 2016).

Our software can reliably extract plant growth traits, color traits and leaf count based on efficient implementations of validated algorithms centered on state-of-the-art methods of image processing and machine learning (Minervini *et al.*, 2014, 2015a; Giuffrida *et al.*, 2015), which are designed to provide robustness to variable experimental settings and perform well with 2D fixed-focus imaging. Although leaf count has also been used previously as a phenotypic parameter (Jansen *et al.*, 2009; Arvidsson *et al.*, 2011), here we adopt a learning-based object counting method for plant leaves using affordable 2D-based vision without the need for expensive (and low-throughput without actuation) 3D vision (Apelt *et al.*, 2015).

To provide a reference of the computational time required by our image-analysis software, on a local workstation (Intel Xeon CPU 3.50 GHz, 64 GB RAM and running Linux) the extraction of plant segmentation and morphological traits took about 5.5 seconds per tray image (24 plants). Training the leaf-counting model on a data set composed of 200 single plant images required ~3.5 min. Predicting the number of leaves of a plant using the learned model took less than a second per plant image.

Central to our software design and machine learning is the notion of training (annotated) data to learn from. We use them to learn how to count leaves for a specific plant species, and also to optimize parameters to make the algorithms adapt to new experimental settings, relieving the user from manually tuning parameters. To help alleviate the process of creating annotated data we also provide an interactive tool for plant- and leaf-level annotations that uses state-of-the-art image processing techniques to minimize expert input (Minervini *et al.*, 2015a). We observed that annotating plant leaves using our tool (the by-products of which include leaf count and plant segmentation) requires on average less than 3 min, in contrast with a completely manual approach requiring on average 30 min for a trained operator to annotate a single plant. Annotating only for the purpose of leaf counting (which involves clicking on each leaf, to help mental memory) takes ~1 min per plant.

Phenotiki has been primarily tested on Arabidopsis; however, with its open architecture and choice of algorithm design, we envision that with suitable choices of

algorithm parameters[3] the Phenotiki platform could also be used to image and extract traits in other plant species. To provide guidance we discuss briefly this potential. The plant segmentation algorithm and the leaf annotation tool are agnostic to plant shape, and could potentially be used for plants with different structure than Arabidopsis. In fact, the annotation tool was also evaluated also on publicly available tobacco plant data (Minervini *et al.*, 2015a). The leaf counting method in its current form relies on the radial arrangement of leaves to learn the model, so it could potentially be used for other plants with radial arrangement of leaves (as evidence from an open challenge on publicly available data suggest; Giuffrida *et al.*, 2015). Overall, we anticipate that our methods can be used with different imaging settings (e.g. different scene background, different field of view, and others), as long as adequate feature resolution is present.

Currently, a fully automated leaf segmentation algorithm is not yet available in Phenotiki, which might be necessary for investigations into differential leaf growth; however, a suitable surrogate could be obtained with counting as performed in this article, which could be used to assess plant status and leaf emergence (Apelt *et al.*, 2015). On the other hand, the interactive annotation tool can also be used for semi-automated leaf segmentation, and we are working towards propagating information for subsequent images in the time-lapse series to reduce user interaction. More encouraging are the findings of a recent collation study and more recent papers using open access data (Minervini *et al.*, 2016) on automated leaf segmentation (Pape and Klukas, 2015; Scharr *et al.*, 2016) and other studies (Tessmer *et al.*, 2013; Yin *et al.*, 2014), which in the future could be integrated in our platform. The results reported show a promising average of 70% accuracy in leaf segmentation on the basis of single 2D images.

We envision the emergence of a community that supports and fosters the continued development of the system, and thanks to the modular design of our framework, user contributions will evolve the device and software to match the needs of diverse and specialized applications. To further facilitate development, parts of our data and expert annotations are available openly (Minervini *et al.*, 2016) and have already been used by the broad image-analysis community (Pape and Klukas, 2015; Romera-Paredes and Torr, 2016; Scharr *et al.*, 2016).

In conclusion, Phenotiki offers a complete hardware and software solution to affordable phenotyping, offering an out-of-box experience. By relying on open software and open hardware we hope to lower the entry barrier and promote the adoption of image-based phenotyping technologies.

[3]We offer a grid search module that helps to find a suitable set of parameters using some annotated data.

EXPERIMENTAL PROCEDURES

Plants and growth conditions

The experimental set-up included the following Arabidopsis lines: ecotype Col-0 (five subjects), *pgm* (plastidial phosphoglucomutase, N210; five subjects), *ctr1* (constitutive triple response 1, N8057; five subjects), *ein2.1* (ethylene insensitive 2.1, N65994; five subjects) and *adh1* (alcohol dehydrogenase 1, N552699; four subjects). Plants were grown in individual pots under a 12-h light/12-h dark regime; artificial daylight illumination was provided by cool-white fluorescent lamps (~100 μmol photons m^{-2} s^{-h} light intensity). Temperature was on average ~22°C (daytime) and ~16°C (nighttime). Watering was provided twice a week by subirrigation. Pots were spaced out in the tray to prevent adult plants from touching. The arrangement of genotypes in the tray was randomized to eliminate possible bias in the results caused by variations in watering or lighting conditions (Figure 2b). No treatments were performed.

The Phenotiki device

Our affordable and compact device (Figures 1a and S1) is based on the Raspberry Pi single-board computer (http://www.raspberrypi.org) used to control an OmniVision OV5647 fixed-optics complementary metal-oxide semiconductor (CMOS) camera sensor (known as RaspiCam), with the ability to capture 5-megapixel static images of the scene (Figure 2a) in the visible spectrum (i.e. RGB color images). A complete list of the equipment used to set up the Phenotiki device and corresponding operating specifications are provided in Appendix S1. Although we used the Raspberry Pi 1 model B, more recent versions with higher computational power are also available at the same cost. In addition, the new RaspiCam V2 version offers higher resolution (8 megapixels). Other types of sensors (e.g. a higher grade camera or environmental monitoring sensors) can be directly attached to the Raspberry Pi via Universal Serial Bus (USB) or General-Purpose Input/Output (GPIO). To facilitate the configuration and monitoring of the device, we deployed a web-based graphical user interface to operate it remotely from a laptop or a smartphone (Figures 1b and S2; Video clip S1). To reduce storage requirements without affecting phenotyping accuracy (Minervini *et al.*, 2015c), images were encoded at the device using the lossless compression standard available in the PNG file format (although Phenotiki supports a variety of lossless and lossy image formats). At the end of the experiment, a ZIP archive containing all of the images acquired was automatically created on the Phenotiki device, and via the web-based interface of the device we downloaded it to a local workstation for storage and processing (Figure S2). Phenotiki can also directly upload data to CyVerse (with additional options such as upload to FTP servers or Cloud storage services in development).

Imaging configuration and set-up

The Phenotiki device was placed approximately 1 m above the plants, affixed via zip-ties on the framework of our chamber. On the basis of a calibration scale we measured an effective pixel resolution of 0.323 mm. At this distance a maximum of 60 Arabidopsis plants grown in pots can be imaged (or up to 80 Arabidopsis rosettes in juvenile stages of development). To obtain consistent color information, a white reference card was included to perform automatic white balancing upon image acquisition.

In addition, another higher grade camera (Canon PowerShot SD1000, shorthanded as Canon) was also used that had movable optics and could adjust the field of view via optical zoom. This sensor was set to image at an effective distance of 50 cm, which is common in growth chambers. This effective distance also dictated the number (24) of subjects used in this study. The diameter of each plant was manually measured with a caliper and recorded on a daily basis for reference.

Image-analysis protocol

The acquired imaging data were processed using our image-analysis software, which has been designed to operate on images showing a top view on rosette-shaped plants and relies on the algorithm by Minervini *et al.* (2014). To isolate plants from the background – a process known as segmentation – the algorithm first automatically localizes plant objects in the tray by placing a bounding box around each plant, and then each plant is segmented from the background. To enable association across time, plants from consecutive images are matched (i.e. tracked). Segmenting plants in images acquired in a general laboratory setting can be a challenging task under typical growth-chamber conditions (e.g. with green algae growing on the soil surface, water reflections, light inhomogeneity, and changes in color and appearance of the plants as a result of senescence or treatments); therefore, the adopted algorithm relies on machine learning and a probabilistic (prior-driven) level set-based active contour model for accurate plant segmentation that can adapt to scene variability (Minervini *et al.*, 2014). As the algorithm requires the tuning of several parameters to achieve this adaptation, we provided a pre-annotated tray image, via a semi-automated tool, upon which the algorithm automatically finds optimal parameters (Appendix S2). We applied the algorithm and found parameters on the images of the experiment and we extracted a variety of traits to describe rosette size (area, diameter, perimeter), morphology (compactness, stockiness), growth stage progression (leaf count), and color, obtaining for each plant a multivariate temporal description of its visual phenotype. For leaf count, we extended a state-of-the-art method that predicts automatically the number of visible rosette leaves (Giuffrida *et al.*, 2015). This learning-based approach requires a set of annotated training images of single isolated plants and corresponding integer number of visible leaves (i.e. the actual per-image leaf count). Given a set of training images, the algorithm learns the features (templates composed of square patches) and a regression model to predict the number of leaves. As the original algorithm by Giuffrida *et al.* (2015) was designed to be agnostic to scale (in order to accommodate the variable distance between sensor and camera of the images in the challenge data set, by design; Table S4), and was tested on a challenge data set that did not provide genotype information, we added two extra features: plant genotype (categorical variable) and projected leaf area (PLA, continuous variable). These properties provide information related to the typical temporal growth behavior, or more generally speaking the dose-response characteristics of each plant, to the algorithm (Poorter *et al.*, 2013). The categorical genotype variable was encoded as five separate dummy variables. Note that the method does not use the actual genotype information per se (e.g. does not know that the first dummy is Col-0). The new features vector is then standardized by subtracting the mean and dividing by the standard deviation. (Further parameter settings are shown in Table S4.)

To facilitate adoption, our image analysis solution is publicly available as a stand-alone MATLAB-based tool (albeit no MATLAB installation or license is required), and is accompanied by an easy-to-use and intuitive graphical user interface (Figures 1c and S3; Video clip S2), and also as a web application running on the CyVerse Cloud (Figures 1d and S4; Video clip S3). The software offers the possibility to analyze image data sets and export or visualize phenotypic results. Additionally, annotation tools are available for the user to provide feedback or labeled data (e.g. segmented plants or number of leaves), which are used to train the models of the learning components in the image-analysis pipeline. All code is open source.

The Phenotiki software was designed in a modular fashion. In the stand-alone version, the user is presented with an integrated view in which several modules are available to address a variety of tasks. The modules communicate via a shared data structure (Figure S9) encapsulating all the metadata associated with an experiment (e.g. subjects, genotypes, acquisition time, user annotations), and populated or augmented with analysis results (e.g. plant segmentation masks, phenotype descriptors) obtained after a module execution. The Cloud-based version of the Phenotiki software follows a similar design, with the modules integrated in a composite application within the BisQue framework (Goff *et al.*, 2011).

ACKNOWLEDGEMENTS

This work was partially supported by a Marie Curie Action: 'Reintegration Grant' (256534) of the European Union's FP7. We thank Nirav Merchant for providing us with access to the CyVerse platform, and the support of Kristian Kvilekval and Dmitry Fedorov for helping us to integrate our software within BisQue. We acknowledge the help of Fabiana Zollo in the implementation on BisQue. Finally, we thank Hanno Scharr, Alistair McCormick and Antonio Masi for providing feedback on the manuscript. The authors declare no conflicts of interest.

SUPPORTING INFORMATION

Additional Supporting Information may be found in the online version of this article.

Figure S1. Pictures of the proposed affordable Phenotiki device.

Figure S2. Screen captures of our web-based software tool to configure and operate the Phenotiki device.

Figure S3. Screen captures showing the user interface of our stand-alone plant image analysis software.

Figure S4. Screen captures of our suite of web-based applications for plant image analysis on the CyVerse cloud platform.

Figure S5. Illustration of some of the visual traits extracted by our system.

Figure S6. Richards' growth curve fitted to the PLA data for each genotype.

Figure S7. Bland–Altman plot showing the agreement between rosette diameter measured with Phenotiki and manually with a caliper.

Figure S8. Agreement between rosette diameter measured automatically from images acquired with a Canon camera and manually with a caliper.

Figure S9. Data structure adopted in the PHENOTIKI analysis software.

Table S1. Parameter estimates of the Richards' growth curve fitted to PLA data.

Table S2. Pairwise comparisons of PLA results between Col-0 and the other genotypes.

Table S3. Pairwise comparisons of leaf count results between Col-0 and the other genotypes.

Table S4. Parameter-setting for the automatic leaf-counting algorithm.

Appendix S1. List of hardware equipment used to set-up the Phenotiki device.

Appendix S2. Additional description of the PHENOTIKI image-analysis software.

Appendix S3. Overview of the computer vision approaches adopted in the PHENOTIKI image analysis software.

Appendix S4. Plant visual trait descriptors extracted by PHENOTIKI.

Appendix S5. Parametric growth analysis based on Richards' curve.

Appendix S6. Power spectral density estimation of the PLA data, highlighting daily cyclic growth patterns.

Video clip S1. Demo of the web-based software to configure the Phenotiki device.

Video clip S2. Demo of the stand-alone PHENOTIKI image-analysis software.

Video clip S3. Demo of the PHENOTIKI image-analysis modules on BisQue/CyVerse.

REFERENCES

Apelt, F., Breuer, D., Nikoloski, Z., Stitt, M. and Kragler, F. (2015) Phytotyping 4D: a light-field imaging system for non-invasive and accurate monitoring of spatio-temporal plant growth. *Plant J.* **82**, 693–706.

Arvidsson, S., Pérez-Rodríguez, P. and Mueller-Roeber, B. (2011) A growth phenotyping pipeline for *Arabidopsis thaliana* integrating image analysis and rosette area modeling for robust quantification of genotype effects. *New Phytol.* **191**, 895–907.

Bland, J.M. and Altman, D.G. (2007) Agreement between methods of measurement with multiple observations per individual. *J. Biopharm. Stat.* **17**, 571–582.

Bours, R., Muthuraman, M., Bouwmeester, H. and van der Krol, A. (2012) OSCILLATOR: a system for analysis of diurnal leaf growth using infrared photography combined with wavelet transformation. *Plant Methods*, **8**, 1–12.

Boyes, D.C., Zayed, A.M., Ascenzi, R., McCaskill, A.J., Hoffman, N.E., Davis, K.R. and Görlach, J. (2001) Growth stage-based phenotypic analysis of Arabidopsis. *Plant Cell*, **13**, 1499–1510.

Brown, T.B., Cheng, R., Sirault, X.R.R., Rungrat, T., Murray, K.D., Trtilek, M., Furbank, R.T., Badger, M., Pogson, B.J. and Borevitz, J.O. (2014) TraitCapture: genomic and environment modelling of plant phenomic data. *Curr. Opin. Plant Biol.* **18**, 73–79.

Carrasco, J.L., Phillips, B.R., Puig-Martinez, J., King, T.S. and Chinchilli, V.M. (2013) Estimation of the concordance correlation coefficient for repeated measures using SAS and R. *Comput. Methods Programs Biomed.* **109**, 293–304.

Caspar, T., Huber, S.C. and Somerville, C. (1985) Alterations in growth, photosynthesis and respiration in a starchless mutant of *Arabidopsis thaliana* (L.) Heynh deficient in chloroplast phosphoglucomutase activity. *Plant Physiol.* **79**, 11–17.

De Vylder, J., Vandenbussche, F., Hu, Y., Philips, W. and Van Der Straeten, D. (2012) Rosette Tracker: an open source image analysis tool for automatic quantification of genotype effects. *Plant Physiol.* **160**, 1149–1159.

Easlon, H.M. and Bloom, A.J. (2014) Easy Leaf Area: automated digital image analysis for rapid and accurate measurement of leaf area. *Appl. Plant Sci.* **2**, 1–4.

Furbank, R.T. and Tester, M. (2011) Phenomics – technologies to relieve the phenotyping bottleneck. *Trends Plant Sci.* **16**, 635–644.

Giuffrida, M.V., Minervini, M. and Tsaftaris, S.A. (2015) Learning to count leaves in rosette plants. In *Proceedings of the Computer Vision Problems in Plant Phenotyping (CVPPP) Workshop* (Tsaftaris, S.A., Scharr, H. and Pridmore, T., eds). BMVA Press, pp. 1.1–1.13.

Goff, S.A., Vaughn, M., McKay, S. *et al.* (2011) The iPlant Collaborative: cyberinfrastructure for plant biology. *Front. Plant Sci.* **2**, 1–16.

Granier, C., Aguirrezabal, L., Chenu, K. *et al.* (2006) PHENOPSIS, an automated platform for reproducible phenotyping of plant responses to soil water deficit in *Arabidopsis thaliana* permitted the identification of an accession with low sensitivity to soil water deficit. *New Phytol.* **169**, 623–635.

Green, J.M., Appel, H., Rehrig, E.M., Harnsomburana, J., Chang, J.F., Balint-Kurti, P. and Shyu, C.R. (2012) PhenoPhyte: a flexible affordable method to quantify 2D phenotypes from imagery. *Plant Methods*, **8**, 1–12.

Guzmán, P. and Ecker, J.R. (1990) Exploiting the triple response of Arabidopsis to identify ethylene-related mutants. *Plant Cell*, **2**, 513–523.

Jansen, M., Gilmer, F., Biskup, B. *et al.* (2009) Simultaneous phenotyping of leaf growth and chlorophyll fluorescence via GROWSCREEN FLUORO allows detection of stress tolerance in *Arabidopsis thaliana* and other rosette plants. *Funct. Plant Biol.* **36**, 902–914.

Kieber, J.J., Rothenberg, M., Roman, G., Feldmann, K.A. and Ecker, J.R. (1993) CTR1, a negative regulator of the ethylene response pathway in Arabidopsis, encodes a member of the Raf family of protein kinases. *Cell*, **72**, 427–441.

Leister, D., Varotto, C., Pesaresi, P., Niwergall, A. and Salamini, F. (1999) Large-scale evaluation of plant growth in *Arabidopsis thaliana* by non-invasive image analysis. *Plant Physiol. Biochem.* **37**, 671–678.

Lobet, G., Draye, X. and Périlleux, C. (2013) An online database for plant image analysis software tools. *Plant Methods*, **9**, 1–8.

Minervini, M. and Tsaftaris, S.A. (2013) Application-aware image compression for low cost and distributed plant phenotyping. In *International Conference on Digital Signal Processing (DSP)*. Piscataway, NJ: IEEE, pp. 1–6.

Minervini, M., Abdelsamea, M.M. and Tsaftaris, S.A. (2014) Image-based plant phenotyping with incremental learning and active contours. *Ecological Informatics*, **23**, 35–48.

Minervini, M., Giuffrida, M.V. and Tsaftaris, S.A. (2015a) An interactive tool for semi-automated leaf annotation. In *Proceedings of the Computer Vision Problems in Plant Phenotyping (CVPPP) Workshop* (Tsaftaris, S.A., Scharr, H. and Pridmore, T., eds). BMVA Press, pp. 6.1–6.13.

Minervini, M., Scharr, H. and Tsaftaris, S.A. (2015b) Image analysis: the new bottleneck in plant phenotyping. *IEEE Signal Process. Mag.* **32**, 126–131.

Minervini, M., Scharr, H. and Tsaftaris, S.A. (2015c) The significance of image compression in plant phenotyping applications. *Funct. Plant Biol.* **42**, 971–988.

Minervini, M., Fischbach, A., Scharr, H. and Tsaftaris, S.A. (2016) Finely-grained annotated datasets for image-based plant phenotyping. *Pattern Recogn. Lett.* **81**, 80–89.

Pape, J.M. and Klukas, C. (2015) Utilizing machine learning approaches to improve the prediction of leaf counts and individual leaf segmentation of rosette plant images. In *Proceedings of the Computer Vision Problems in Plant Phenotyping (CVPPP) Workshop* (Tsaftaris, S.A., Scharr, H. and Pridmore, T., eds). BMVA Press, pp. 3.1–3.12.

Perata, P. and Alpi, A. (1993) Plant responses to anaerobiosis. *Plant Sci.* **93**, 1–17.

Poorter, H., Anten, N.P.R. and Marcelis, L.F.M. (2013) Physiological mechanisms in plant growth models: do we need a supra-cellular systems biology approach? *Plant Cell Environ.* **36**, 1673–1690.

Romera-Paredes, B. and Torr, P.H.S. (2016) Recurrent instance segmentation. In *European Conference on Computer Vision (ECCV)* (Leibe, B., Matas, J., Sebe, N. and Welling, M., eds). Berlin: Springer, pp. 312–329.

Rousseau, D., Dee, H. and Pridmore, T. (2015) Imaging methods for phenotyping of plant traits. In *Phenomics in Crop Plants: Trends, Options and Limitations* (Kumar, J., Pratap, A. and Kumar, S., eds). Berlin: Springer, pp. 61–74.

Scharr, H., Minervini, M., French, A.P. *et al.* (2016) Leaf segmentation in plant phenotyping: a collation study. *Mach. Vis. Appl.* **27**, 585–606.

Sozzani, R., Busch, W., Spalding, E.P. and Benfey, P.N. (2014) Advanced imaging techniques for the study of plant growth and development. *Trends Plant Sci.* **19**, 304–310.

Tessmer, O.L., Jiao, Y., Cruz, J.A., Kramer, D.M. and Chen, J. (2013) Functional approach to high-throughput plant growth analysis. *BMC Syst. Biol.* **7**, S17.

Tisné, S., Serrand, Y., Bach, L. *et al.* (2013) Phenoscope: an automated large-scale phenotyping platform offering high spatial homogeneity. *Plant J.* **74**, 534–544.

Tsaftaris, S.A. and Noutsos, C. (2009) Plant phenotyping with low cost digital cameras and image analytics. In *Information Technologies in*

Environmental Engineering (Athanasiadis, I.N., Rizzoli, A.E., Mitkas, P.A. and Gómez, J.M., eds). Berlin: Springer, pp. 238–251.

Tsaftaris, S.A., Minervini, M. and Scharr, H. (2016) Machine learning for plant phenotyping needs image processing. *Trends Plant Sci.* **21**, 989–991.

Walter, A., Scharr, H., Gilmer, F. *et al.* (2007) Dynamics of seedling growth acclimation towards altered light conditions can be quantified via GROWSCREEN: a setup and procedure designed for rapid optical phenotyping of different plant species. *New Phytol.* **174**, 447–455.

Wiese, A., Christ, M.M., Virnich, O., Schurr, U. and Walter, A. (2007) Spatio-temporal leaf growth patterns of *Arabidopsis thaliana* and evidence for sugar control of the diel leaf growth cycle. *New Phytol.* **174**, 752–761.

Yin, X., Liu, X., Chen, J. and Kramer, D.M. (2014) Multi-leaf tracking from fluorescence plant videos. In *International Conference on Image Processing (ICIP)*. Piscataway, NJ: IEEE, pp. 408–412.